Reservoir engineering for maximally efficient quantum engines

Taysa M. Mendonça,[1] Alexandre M. Souza,[2] Rogério J. de Assis,[3] Norton G. de Almeida,[3] Roberto S. Sarthour,[2] Ivan S. Oliveira,[2] and Celso J. Villas-Boas[1]

[1]*Departamento de Física, Universidade Federal de São Carlos, 13565-905, São Carlos, São Paulo, Brazil*

[2]*Centro Brasileiro de Pesquisas Físicas, 22290-180, Rio de Janeiro, Rio de Janeiro, Brazil*

[3]*Instituto de Física, Universidade Federal de Goiás, 74001-970, Goiânia, Goiás, Brazil*

(Received 18 February 2020; accepted 18 November 2020; published 24 December 2020)

We employ reservoir engineering technique to build an artificial thermal bath at arbitrary (effective) negative and positive temperatures for a single spin system. The required interaction engineering is achieved by applying a specific sequence of radio-frequency pulses using nuclear magnetic resonance, while the temperature of the bath can be controlled by appropriate preparation of the initial ^{1}H nuclear spin state. This artificial reservoir allowed us to implement a single qubit quantum engine that operates at a single reservoir at effective negative temperature and with maximum efficiency, independent of the unitary transformation performed on the qubit system, as long as it changes the qubit state. We measured the population of the carbon spin and the efficiency of our quantum engine, which are in very good agreement with the predicted results.

DOI: 10.1103/PhysRevResearch.2.043419

I. INTRODUCTION

The study of quantum thermodynamics has been growing in recent years since it has allowed a deeper understanding of the basic laws of thermodynamics and their limitations that appear when quantum effects are taken into account [1]. In this context, quantum engines, which employ quantum systems as the working medium, have attracted great interest from physicists since they allow investigating the fundamental limits of quantum engine efficiencies [2,3]. In a recent work we have shown that quantum engines working with one of the reservoirs at an effective negative temperature [4–7] present counterintuitive behaviors as higher efficiency when performing nonadiabatic cycles [8], contrary to the usual behavior of classic machines which provide their maximum efficiency only in strictly adiabatic processes. In Ref. [8] the temperature of the working medium is simulated by properly preparing the qubit in a thermal state. So, the natural question is: can we indeed prepare a real reservoir with arbitrary temperature, even an effective negative one, for nuclear magnetic resonance (NMR) systems? By employing reservoir engineering techniques [9,10], which were already successfully applied to a large number of different systems [11–20], here we show that this is indeed possible. Following these ideas, here we show how to engineer reservoirs at arbitrary temperatures for a qubit spin system, even at effective negative ones [4–7], which allows for intriguing phenomena in quantum engines [8]. As a special application of reservoirs at effective negative temperatures, here we implement a single qubit quantum engine, which presents the advantage of employing a single reservoir and allowing for maximum efficiency (100%), independently of the unitary transformation we carry out on the working medium, as long as it changes its state.

This paper is organized as follows: In Sec. II we present a description of our physical system, in Sec. III we describe the dynamics of the effective Hamiltonian after the reservoir engineering process, in Sec. IV we present the experimental results obtained for the thermalization of a qubit coupled to engineered thermal reservoirs with different temperatures. As a proof of concept, in Sec. V we built a quantum thermal engine that works with a single reservoir allowing maximum efficiency and, finally, in Sec. VI we present our concluding remarks. In the appendices we give details of the derivations of the effective Hamiltonian, fidelity of the experimental data, calculation of work and heat and, finally, we checked the gain/loss of energy from the hydrogen bath during the unitary evolution applied in each cycle of our quantum engine.

II. SYSTEM

Our system is composed by an adamantane molecule $C_{10}H_{16}$, Fig. 1(a), which contains six CH_2 groups and four CH groups. In our model, the qubit system is the carbon spin from the CH_2 group, whose signal can be well isolated in the NMR spectrum, as shown in Fig. 1(a), since the signals appear according to the neighborhood of each spin, thus resulting, in our case, in two signals for carbon spin, one for carbon bound to one hydrogen and the other for carbon bound to 2 hydrogens. The ^{13}C nuclear spins ($S = 1/2$) are approximately 1.1% of all the carbon spins contained in an adamantane sample while ^{1}H ($I = 1/2$) has a natural abundance of 99.98%, therefore, in an approximation we have 1 ^{13}C spin for 160 ^{1}H spins. Thus, the large amount of ^{1}H spins around a single ^{13}C spin allows us to say that hydrogens work out as a spin bath for ^{13}C. We can disregard the carbon-carbon interaction

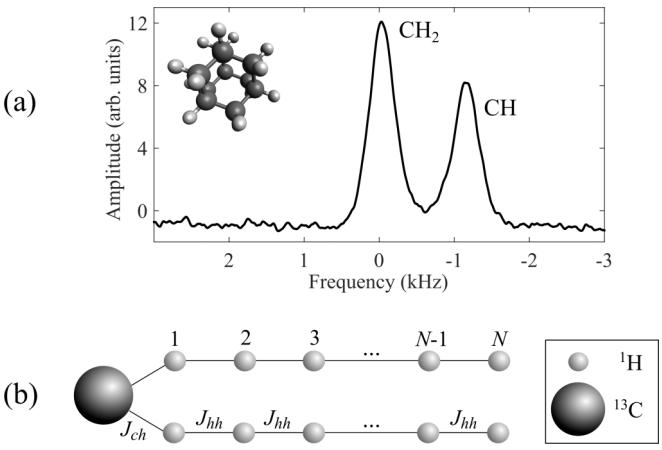

FIG. 1. Spin system: (a) The NMR spectrum of the ^{13}C nuclear spin in a sample of polycrystalline of adamantane. (b) Representation of our spin system model composed by a ^{13}C atom coupled to two linear chains of N ^{1}H atoms each.

and, although a carbon spin couples with several ^{1}H spins close to it, the coupling strength is inversely proportional to the distance between the respective spins, which allow us to keep only the first-neighbor interactions. Therefore, we can consider each ^{13}C nucleus as an independent spin surrounded by a large number of hydrogen nuclear spins that acts as a bath to the carbons [21–23]. For modeling the entire spin system, here we propose a configuration with a ^{13}C linked to 2 chains of ^{1}H, as illustrated in Fig. 1(b).

The experiments were performed at room temperature with a sample of polycrystalline adamantane subjected to a high intensity static magnetic field and radiofrequency pulses using a Varian 500 MHz NMR spectrometer. We consider $\boldsymbol{S} = S_x\boldsymbol{i} + S_y\boldsymbol{j} + S_z\boldsymbol{k}$ and $\boldsymbol{I} = I_x\boldsymbol{i} + I_y\boldsymbol{j} + I_z\boldsymbol{k}$ as the nuclear spin operators for ^{13}C and ^{1}H, respectively. In polycrystalline adamantane the spin-spin interaction is dominated by the dipolar interaction [24,25], while the interaction of the spins with the static magnetic field results in a Zeeman splitting. The Larmor frequencies in our experiment are 125 and 500 MHz for the ^{13}C and ^{1}H, respectively. Using the secular approximation, we can neglect the terms of the dipolar coupling Hamiltonian that do not commute with the strong Zeeman interaction [24].

III. DYNAMICS

The total Hamiltonian for this model written in the rotating frame at the Larmor frequencies is of the form $H = H_{SE} + H_E$ [25], where H_{SE} and H_E are, respectively, the Hamiltonians of the system-environment interaction and of the environment, such that

$$H_{SE} = J_{ch} \sum_{\alpha=a,b} S_z I_z^{\alpha,1}, \tag{1}$$

$$H_E = J_{hh} \sum_{\alpha=a,b} \sum_{k=1}^{N-1} \left[2I_z^{\alpha,k} I_z^{\alpha,k+1} - \left(I_x^{\alpha,k} I_x^{\alpha,k+1} + I_y^{\alpha,k} I_y^{\alpha,k+1}\right)\right], \tag{2}$$

where the index $\alpha = a, b$ represents the arrays of hydrogen spins, being the first one of each array coupled directly to the ^{13}C. The index k represents the k^{th} ^{1}H of the bath, $2N$ being the total number of ^{1}H nuclear spins in the bath system (N in each array). J_{ch} and J_{hh} are, respectively, the carbon-hydrogen and hydrogen-hydrogen coupling constants.

The natural interaction between carbon and hydrogen is described as an Ising model, therefore, it is not capable of promoting inversions in the qubit system (spin carbon) state, therefore, it is not immediately useful for our proposal. We need an interaction like the Heisenberg model, that is, an interaction that allows the exchange of energy between the system and the environment. To have this interaction model we need to do a reservoir engineer, that is, we need to manipulate the nuclear spin interactions in order to obtain an effective suitable Hamiltonian. This can be done by applying a sequence of radio frequency (r.f.) pulses (hard pulses) with duration time τ_p, with each one followed by a free evolution governed by the system Hamiltonian H during a short time interval Δt (free evolution time). This sequence (total duration τ_c) is then described by the evolution operator

$$U(\tau_c) = e^{-\frac{i}{2\hbar}H\Delta t} P_4 e^{-\frac{i}{\hbar}H\Delta t} P_3 e^{-\frac{i}{\hbar}H\Delta t} P_2 e^{-\frac{i}{\hbar}H\Delta t} P_1 e^{-\frac{i}{2\hbar}H\Delta t}, \tag{3}$$

where $P_1 = \exp[-i\frac{\pi}{2}(S_x + I_x)]$, $P_2 = \exp[i\frac{\pi}{2}(S_x + I_x)]$, $P_3 = \exp[-i\frac{\pi}{2}(S_y + I_y)]$, and $P_4 = \exp[i\frac{\pi}{2}(S_y + I_y)]$ are r.f. pulse operators that make the spins I and S to flip at angles $\pi/2$ in the x, $-x$, y and $-y$ directions, respectively. We can rewrite Eq. (3) as a single evolution operator governed by an effective Hamiltonian, i.e., $U(t) = e^{-\frac{i}{\hbar}H_{\text{eff}}t}$, which can be calculated using average Hamiltonian theory [25]. The effective Hamiltonian reads (see Appendix A for the detailed derivation)

$$H_{\text{eff}}^{SE} \simeq J_{ch}^{\text{eff}} \sum_{\alpha=a,b} \left(2S_z I_z^{\alpha,1} + S_x I_x^{\alpha,1} + S_y I_y^{\alpha,1}\right), \tag{4}$$

$$H_{\text{eff}}^{E} \simeq J_{hh}^{\text{eff}} \sum_{\alpha=a,b} \sum_{k=1}^{N-1} \left[2I_z^{\alpha,k} I_z^{\alpha,k+1} - \left(I_x^{\alpha,k} I_x^{\alpha,k+1} + I_y^{\alpha,k} I_y^{\alpha,k+1}\right)\right], \tag{5}$$

where $J_{ch}^{\text{eff}} = J_{ch}/4$ and $J_{hh}^{\text{eff}} = J_{hh}/4$ is the effective coupling constants of the interactions between the nuclear spin of the ^{13}C and its first neighboring hydrogens, and between the nuclear hydrogen spins of each chain, respectively, obtained after the application of the pulse sequence described in Eq. (3). As the duration of the r.f. pulses (τ_p) is fixed, we can optimize the time interval (Δt) between them to minimize the decoherence effects. As shown in Appendix A, the shorter the time interval Δt, the better the accuracy of the dynamics predicted by the effective Hamiltonian.

The control of the spin temperature is done by adjusting the hydrogen nuclear spin state [3,4,6,26]. To study the dynamics and thermalization of the carbon spin system, we solve the time-dependent Schrödinger equation numerically considering different sizes of the environment and different initial states. Figure 2(a) shows how the dynamics of our carbon spin system behaves when we increase the size of the environment (number of hydrogen spins) when the carbon spin system is prepared in the excited state $|1\rangle$ and the environment spins at

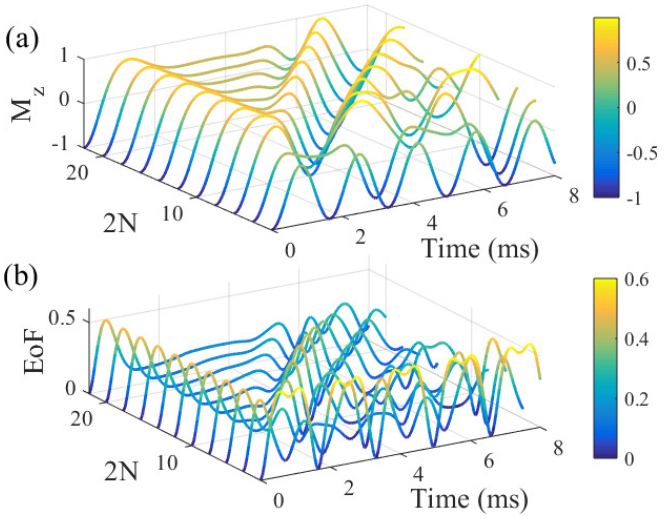

FIG. 2. (a) z component of the magnetization of the carbon nuclear spin as a function of time and number of qubits of the bath derived via solution of the Schrödinger equation with H_{eff} and (b) EoF between the carbon and first hydrogen spin (first array). The initial state is $|1\rangle$ for the carbon nuclear spin and $|0\rangle$ for all hydrogen spins ($T = 0$ K). The parameters used here are $J_{ch}^{\text{eff}} = 550$ rad s^{-1} and $J_{hh}^{\text{eff}} = 980$ rad s^{-1}.

$T = 0$ K, i.e., all of them in the ground state $|0\rangle$. We observe that the greater the number of hydrogens in the spin system, the better the thermalization. In all simulations we use the coupling strengths $J_{ch}^{\text{eff}} = 550$ rad s^{-1} and $J_{hh}^{\text{eff}} = 980$ rad s^{-1}, this values were calibrated from the experimental data shown in Fig. 3. In Fig. 2(b) we also plot the degree of entanglement between the carbon and the first hydrogen spin (first array), quantified by the entanglement of formation (EoF) [27]. We can see that entanglement moves to the other hydrogen spins, disentangling the carbon spin from the hydrogen chains,

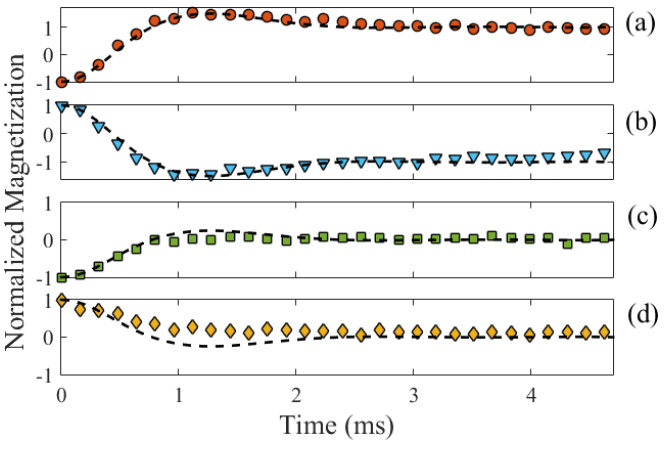

FIG. 3. Normalized z component of the magnetization of the carbon nuclear spin (M_z) as a function of time for the initial states: (a) Carbon in $|1\rangle$ and hydrogens in $|0\rangle$; (b) Carbon in $|0\rangle$ and hydrogens in $|1\rangle$; Hydrogens in $\rho = \frac{1}{2}(|0\rangle\langle 0| + |1\rangle\langle 1|)$ and carbon in (c) $|1\rangle$ and (d) $|0\rangle$. The symbols refer to experimental data while the dashed lines are derived theoretically via H_{eff} (with $2N = 22$ hydrogen spins). The parameters used here are $J_{ch}^{\text{eff}} = 550$ rad s^{-1} and $J_{hh}^{\text{eff}} = 980$ rad s^{-1}.

at the same time, the state of the carbon spin approaches the initial hydrogen spin state; this is a clear signature that the hydrogen spin chains work out as a real thermal bath for the carbon spin, as desired. As the dimension of the system wave vector scales as 2^M, where $M = 2N + 1$ is the total number of spins in our system; our numerical simulations were limited to $M = 23$ spins due to our computational resources. A way to circumvent this problem would be by employing the mean field approximation, however, this approximation is not able to describe the creation of quantum correlations between the spins, which is a key aspect of our reservoir engineering.

IV. EXPERIMENTAL RESULTS

We prepared different initial states for ^{13}C and ^{1}H simulating different temperatures of the spin bath for the main qubit (carbon spin) and measured the expected value of the z component of magnetization. Initially we start from the thermal equilibrium at room temperature, in the high-temperature limit, and the spin states are almost equally populated with the excess of the lower energy state on the order of 10^{-5}. First the carbon spins are prepared in the excited state $|1\rangle$ (negative temperature) and the hydrogen spins are kept in the thermal equilibrium state (ground state $|0\rangle$ or positive temperature), Fig. 3(a). Then we prepared carbon spins in the state $|0\rangle$ and the hydrogen spins in the thermal equilibrium with negative temperature (state $|1\rangle$), Fig. 3(b), and the resulting situation is equivalent to put the carbon spins in contact with a thermal bath with negative temperature. Still in Fig. 3, we do the same for the bath at infinite temperature, i.e., the hydrogen spins of the bath are prepared in the mixed state without population excess $\rho = \frac{1}{2}(|0\rangle\langle 0| + |1\rangle\langle 1|)$, Figs. 3(c) and 3(d). The experimental data are normalized according to the magnetization of the carbon spin after a $\pi/2$ pulse. During the thermalization process, polarization formed hydrogen spins can be transferred to carbons, this causes the magnetization to exceed the $+1$ and -1 values. Where there are negative values means that the magnetization is in the opposite direction in relation to the magnetization with positive values. To reproduce the polarization in the simulations, all results were normalized and all theoretical lines were multiplied by the same factor of 1.38. Finally, we could observe that the qubit system tends to thermalize in the state of the qubits bath, and this happens even when the qubit system is in the ground state and the qubits bath are in the excited state.

A slight difference between experimental and theoretical data can be observed in different regions in all panels of Fig. 3, however, all results show good fidelity (see Appendix B). The origin of these errors are mainly due to r.f. pulse imperfections and the natural relaxation of the spins. In NMR, the thermal relaxation time is associated with the spin-lattice relaxation, which occurs at a characteristic times T_1, which for our system are $T_1^H = 0.9$ s and $T_1^C = 1.6$ s. Despite being a nonequilibrium reservoir, note that the entire process of thermalizing the qubit system with the reservoir occur in a time on the order of a few milliseconds, a time small enough to neglect the sample's relaxation effects. We can, therefore, consider that the operation of our quantum engine happens in local equilibrium, enforcing the laws of classical thermodynamics.

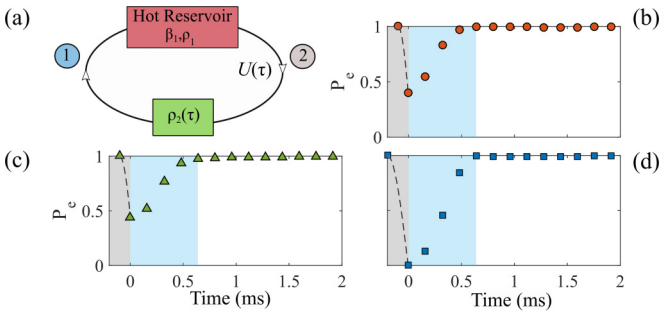

FIG. 4. (a) Scheme of the cycle of a single reservoir in which step 1 corresponds to the unitary evolution and the step 2 corresponds to the thermalization step with the reservoir with negative temperature. Population (P_e) of the excited state as a function of time for different unitary operations. We consider the beginning of our cycle in $t = 0$, starting from a thermalized state with the environment at a negative effective temperature. The unitary operations performed were: (b) $U_x = \exp(-i\frac{\pi}{2}S_x)$, (c) $U_y = \exp(-i\frac{\pi}{2}S_y)$, (d) $U_\pi = \exp(-i\pi S_x)$. The work is calculated in the unitary operation region (gray region) and the heat exchanged with the hot thermal reservoir is calculated from the thermalization region with the reservoir (blue region).

V. QUANTUM ENGINE OF A SINGLE RESERVOIR

By employing the previously engineered reservoir, here we perform a single reservoir quantum engine. The key ingredient to this end is the preparation of the reservoir at an effective negative temperature, in this case the quantum engine always turns all absorbed heat from the hot reservoir into net work. If the reservoir has a positive temperature, the quantum engine will always turn all net work into heat when it comes in contact with the hot reservoir (see proof in the Appendix C). The spin 1/2 of the ^{13}C nucleus is the working medium, and the ensemble of spin 1/2 of ^{1}H nuclei plays the role of the hot thermal reservoir. The following relation describes the relevant steps of our experiment:

$$\rho_{\text{ground}} \overset{\text{thermalization}}{\rightarrow} \rho_1 \overset{U(\tau)}{\rightarrow} \rho_2 \overset{\text{thermalization}}{\rightarrow} \rho_1, \tag{6}$$

and the scheme of the thermodynamic cycle corresponding to our quantum engine is described in Fig. 4(a).

First the qubit system (carbon nucleus) is put in contact with the hot reservoir, to absorb heat from it [a step described in Fig. 3(b), i.e., step $\rho_{\text{ground}} \rightarrow \rho_1$ in relation (6)]. Therefore, the ^{13}C spin will initially be in the thermal state $\rho_1 = e^{-\beta_1 H_1}/Z_1$, where $H_1 = -\frac{1}{2}\hbar\omega_1 S_z$ is the Zeeman Hamiltonian for the carbon nucleus, with $\hbar$ being the Planck's constant and ω_1 is the Larmor frequency of the ^{13}C nuclear spin. Z_1 is the partition function, $\beta_1 = 1/k_B T$ such that $T < 0$ is the spin temperature, and k_B is the Boltzmann constant. Then, our thermodynamic cycle consists of two steps:

(i) First, an unitary evolution operator $U(\tau)$ is applied to bring the ^{13}C spin state to $\rho_2 = U(\tau)\rho_1 U^\dagger(\tau)$ [tep $\rho_1 \rightarrow \rho_2$ in relation (6)].This step is performed when the system qubit is already thermalized with the environment, i.e., the r.f. pulse that simulates a unitary operation is only applied after a time interval five times longer than the relaxation time of the engineered system, that is, when $t \approx 5$ ms. The unitary evolution shown in the gray region of Fig. 4 is only representative since this operation occurs in 32 μs for U_x and U_y and 64 μs for U_π, i.e, much shorter than the typical evolution time of our system. Therefore, we assume the initial time for the thermalization process described in step (ii) as our $t = 0$. More details of this step can be found in Appendix D. In this process the Hamiltonian changes, starting from H_1, assuming a different form at intermediate times $H(t)$, and finally returning to its initial form H_1. In our experiment, the unitary operations were carried out fast enough such that all the variation of the energy of the quantum engine is entirely associated with the variation of the Hamiltonian, thus without heat exchange with the environment. The gray region in Fig. 4(a) refers to the carbon nucleus leaving the thermalized state with the hot reservoir (spin bath) ρ_1 and going to the state $\boldsymbol{\rho_2}$ as a result of the unitary operation. In this case, the work done by/on the quantum engine is given by [28] (see Appendix C for details)

$$\langle W\rangle = \text{Tr}[\rho_2 H_1] - \text{Tr}[\rho_1 H_1] = -\hbar\omega_1\xi\tanh\left(\tfrac{1}{2}|\beta_1|\hbar\omega_1\right), \tag{7}$$

where $\xi = |\langle 1|U(t)|0\rangle|^2 \geqslant 0$ is the transition probability between initial state $|0\rangle$ and $|1\rangle$ and $\beta_1 = -|\beta_1| < 0$. Here $\langle W\rangle < 0$ (>0) means that the work is done by (on) the quantum engine.

(ii) The next step consists of thermalization with the hot thermal reservoir (step $\rho_2 \rightarrow \rho_1$ in relation (6), thus bringing the system back to its initial state), which is related to the blue region in Fig. 4. During this process, the Hamiltonian is kept constant. Thus the variation of the system energy is entirely associated with the heat exchange, $\langle Q\rangle$, with the hot thermal reservoir, which is given by [28] (see Appendix C for details)

$$\langle Q\rangle = \text{Tr}[\rho_1 H_1] - \text{Tr}[\rho_2 H_1] = \hbar\omega_1\xi\tanh\left(\tfrac{1}{2}|\beta_1|\hbar\omega_1\right). \tag{8}$$

In Fig. 4 we show the application of three different unitary operators: Fig. 4(b) $U_x = \exp(-i\frac{\pi}{2}S_x)$, Fig. 4(c) $U_y = \exp(-i\frac{\pi}{2}S_y)$, Fig. 4(d) $U_\pi = \exp(-i\pi S_x)$, where U_x and U_y are operators that represent pulses in the x and y directions, allowing the ^{13}C spin to flip by an angle of $\pi/2$. U_π is the operator that rotates the spin by an angle of π. We also performed a fourth operation $U_I = \exp(-2i\pi S_y) = \mathbb{I}$, where U_I is an identity operator (a complete rotation around the Bloch sphere), which is not shown in Fig. 4. The total magnetization in the x, y, and z directions, $M_U = (M_x, M_y, M_z)$, immediately after each unitary operation (second point in Fig. 4) is $M_{U_x} = (0.11, -0.92, 0.20)$a.u., $M_{U_y} = (0.96, -0.05, 0.13)$a.u., $M_{U_\pi} = (-0.01, -0.01, 1.0)$a.u., and $M_{U_I} = (-0.01, 0.15, -0.87)$a.u. (not shown in Fig. 4).

The results obtained experimentally for the different unitary operations are $\langle W\rangle_{U_x} = -(1.97 \pm 0.28)\mu eV$, $\langle W\rangle_{U_y} = -(1.84 \pm 0.21)\mu eV$, $\langle W\rangle_{U_\pi} = -(3.27 \pm 0.22)\mu eV$, and $\langle W\rangle_{U_I} = -(0.20 \pm 0.21)\mu eV$. The heat absorbed from the reservoir are $\langle Q\rangle_{U_x} = (1.96 \pm 0.29)\mu eV$, $\langle Q\rangle_{U_y} = (1.79 \pm 0.18)\mu eV$, $\langle Q\rangle_{U_\pi} = (3.24 \pm 0.22)\mu eV$, and $\langle Q\rangle_{U_I} = (0.20 \pm 0.21)\mu eV$. Both the work and the heat are calculated by taking into account the carbon spin state prior and after each process, i.e., the unitary evolution and the thermalization with the hot reservoir, respectively, to this end we performed a tomography on the carbon state. Thus, the efficiency $\eta = |\langle W\rangle/\langle Q\rangle|$ for each process is $\eta_{U_x} = 1.00 \pm 0.05$, $\eta_{U_y} = 1.03 \pm 0.06$, $\eta_{U_\pi} = 1.01 \pm 0.02$,

and $\eta_{U_l} = 1.00 \pm 0.12$. Thus, whenever the unitary evolution changes the carbon spin state, there will be a non null heat absorbed from the reservoir and it will be entirely converted into work in the thermodynamic cycle of our quantum engine. In Appendix D we show that there is no significant gain or loss of energy from the hydrogen bath during the unitary evolution applied in each cycle.

VI. CONCLUSION

We have applied the reservoir engineering technique to build up reservoirs with arbitrary temperatures, even effective negative ones, for qubit systems. Our system is composed by a nuclear carbon spin (the main qubit) coupled to a large number of nuclear hydrogen spins. By properly manipulating the initial hydrogen state and the carbon-hydrogen and hydrogen-hydrogen nuclear spin interactions, the effective dynamics describes the interaction of a qubit with reservoirs at arbitrary temperatures. We have shown theoretically that, the larger the number of hydrogen spins, the better the hydrogen arrays work out as a bath for the main qubit, which is in excellent agreement with our experimental results. As an application, we have implemented a single reservoir heat engine. Several papers have discussed how to increase the efficiency of quantum engines, for example via the use of quantum coherence [29,30] or artificial environments as squeezed reservoirs [10,11], however, as we have shown here, the simple use of a single reservoir at negative effective temperature allows us to obtain maximum efficiency ($\eta = 1$) regardless of the unitary transformation performed on the qubit (making sure that the final state is different from the initial one in the unitary transformation), thus being, to the best of our knowledge, the simpleest and most efficient quantum engine implemented so far. Naturally, to reach this result we need to build up this artificial reservoir, with inverted population, which demands energy, but this is the price we have to pay for this achievement. For instance, this is quite similar to what happens to a laser, another system based on inverted population, which is responsible for great scientific and technological advances in the last decades. Notice that, as usually done in other works that also employ artificial reservoirs to improve the efficiency of quantum engines [8,31,32], we did not take into account the work needed to prepare our reservoir. Thus, we believe our single reservoir heat engine can be another interesting application for inverted population systems and that the results presented here can be very useful for investigating fundamental and applications of quantum thermodynamics in general, for instance, to study quantum thermal engines that require specific kinds of reservoirs [8,31].

ACKNOWLEDGMENTS

This work was supported by the Brazilian National Institute of Science and Technology for Quantum Information (INCT-IQ) Grant No. 465469/2014-0 and by the CAPES - Finance Code 001. C.J.V.-B. is also grateful for the support by the São Paulo Research Foundation (FAPESP) Grants No. 2013/04162-5 and No. 2019/11999-5, and the National Council for Scientific and Technological Development (CNPq) Grant No. 307077/2018-7. A.M.S. acknowledges support from the Brazilian agencies FAPERJ (Grant No. 203.166/2017) and CNPq (Grant No. 304986/2016-0). N.G.A. also acknowledges the support by the FAPEG agency.

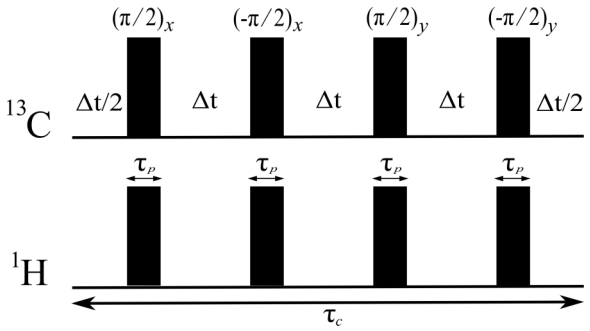

FIG. 5. Sequence of r.f. pulses used to obtain an effective Hamiltonian that allows the exchange of energy between the system and the environment. τ_p is the time of each r.f. pulse, τ_c is the time of a complete cycle of pulses, and Δt is the time between the r.f. pulses.

APPENDIX A: DERIVATION OF THE EFFECTIVE HAMILTONIAN

The interaction between carbon and hydrogen that appears naturally in our system, described in Eqs. (1) and (2), is not interesting in our work because it only causes dephase on the qubit system (carbon spin), being unable to flip the qubit. To solve this, it is necessary to manipulate the nuclear spins in order to obtain an adequate effective Hamiltonian. We do this by applying the r.f. pulse sequence described in Fig. 5.

The time of each pulse τ_p is the time necessary for the spins to rotate by an angle of $\pi/2$ around the Bloch sphere (in x or y directions) when submitted to r.f. pulses with intensities calibrated for each species of spin. Δt is the time between the pulses (free evolution governed by the system Hamiltonian H). The total sequence (duration τ_c) is then given the evolution operator

$$U(\tau_c) = e^{-\frac{i}{2\hbar}H\Delta t}P_4 e^{-\frac{i}{\hbar}H\Delta t}P_3 e^{-\frac{i}{\hbar}H\Delta t}P_2 e^{-\frac{i}{\hbar}H\Delta t}P_1 e^{-\frac{i}{2\hbar}H\Delta t}, \tag{A1}$$

where $P_1 = \exp[-i\frac{\pi}{2}(S_x + I_x)]$, $P_2 = \exp[i\frac{\pi}{2}(S_x + I_x)]$, $P_3 = \exp[-i\frac{\pi}{2}(S_y + I_y)]$, and $P_4 = \exp[i\frac{\pi}{2}(S_y + I_y)]$ are r.f. pulse operators that make the spins I and S to flip at angles $\pi/2$ in the x, $-x$, y, and $-y$ directions, respectively. We can write Eq. (A1) as a single evolution operator, i.e., $U(t) = e^{-\frac{i}{\hbar}H_{\text{eff}}t}$, where H_{eff} is the effective Hamiltonian that can be derived using average Hamiltonian theory [25]:

$$H_{\text{eff}} = \bar{H}_0 + \bar{H}_1 + \bar{H}_2 + \cdots \bar{H}_p. \tag{A2}$$

The terms of H_{eff} can be calculated from the Magnus' expansion [33], where $\bar{H}_0$ is the first approximation for the Hamiltonian and $\bar{H}_1, \bar{H}_2, ..., \bar{H}_p$ are the correction terms [34]. The time interval between the different pulses used in this work is designed to be small enough such that the correction terms are reduced close to zero, remaining only the

zeroth-order term $\bar{H}_0$, which is given by [25]

$$\bar{H}_0 = \frac{1}{t}\sum_{j=1}^{M}\Delta t_j \tilde{H}_j, \tag{A3}$$

where $\tilde{H}_j = T_j^{\dagger} H T_j$, $T_j = \prod_{m=1}^{M} P_m$, and $t = \sum_{j=1}^{M}\Delta t_j$, M being the number of r.f. pulses. Δt_j is the time duration that the system evolves under the $\tilde{H}_j$ Hamiltonian.

From the r.f. pulse sequence (A1) we determine the shape of P_m:

$$T_1 = e^{-i\frac{\pi}{2}S_x}e^{-i\frac{\pi}{2}I_x}, \tag{A4}$$

$$T_2 = e^{i\frac{\pi}{2}S_x}e^{i\frac{\pi}{2}I_x}e^{-i\frac{\pi}{2}S_x}e^{-i\frac{\pi}{2}I_x} = \mathbb{I}, \tag{A5}$$

$$T_3 = e^{-i\frac{\pi}{2}S_y}e^{-i\frac{\pi}{2}I_y}e^{i\frac{\pi}{2}S_x}e^{i\frac{\pi}{2}I_x}e^{-i\frac{\pi}{2}S_x}e^{-i\frac{\pi}{2}I_x} = e^{-i\frac{\pi}{2}S_y}e^{-i\frac{\pi}{2}I_y}, \tag{A6}$$

$$T_4 = e^{i\frac{\pi}{2}S_y}e^{i\frac{\pi}{2}I_y}e^{-i\frac{\pi}{2}S_y}e^{-i\frac{\pi}{2}I_y}e^{i\frac{\pi}{2}S_x}e^{i\frac{\pi}{2}I_x}e^{-i\frac{\pi}{2}S_x}e^{-i\frac{\pi}{2}I_x} = \mathbb{I}. \tag{A7}$$

Then we have

$$\tilde{H}_1 = T_1\sum_{\alpha=a,b}\left\{J_{ch}S_z I_z^{\alpha,1} + J_{hh}\sum_{k=1}^{N-1}\left[2I_z^{\alpha,k}I_z^{\alpha,k+1} - \left(I_x^{\alpha,k}I_x^{\alpha,k+1} + I_y^{\alpha,k}I_y^{\alpha,k+1}\right)\right]\right\}T_1. \tag{A8}$$

Each $\tilde{H}_j$ gives us the evolution of the spin operators contained in the Hamiltonian after each r.f. pulse. A simple way to calculate each evolution is using the equation of motion in magnetism [25], i.e., $^{d\boldsymbol{J}}/_{dt} = \boldsymbol{J}\times\mathbf{H}$. Since $\boldsymbol{\mu} = \gamma\boldsymbol{J}$, $d\boldsymbol{\mu}/dt = \boldsymbol{\mu}\times\mathbf{B}$, that is, the flow variation of the angular momentum is equal to the torque acting on the elementary dipoles. Therefore, we can write, for example, that an evolution of an operator initially in z, after applying a pulse in x, will go in the y direction, i.e., $S_z \times S_x = S_y$. Thus, the result of Eq. (A8) will be

$$\tilde{H}_1 = \sum_{\alpha=a,b}\left(J_{ch}S_y I_y^{\alpha,1} + J_{hh}\sum_{k=1}^{N-1}\left\{2I_y^{\alpha,k}I_y^{\alpha,k+1} - \left[I_x^{\alpha,k}I_x^{\alpha,k+1} + \left(-I_z^{\alpha,k}\right)\left(-I_z^{\alpha,k+1}\right)\right]\right\}\right), \tag{A9}$$

$$\tilde{H}_1 = \sum_{\alpha=a,b}\left\{J_{ch}S_y I_y^{\alpha,1} + J_{hh}\sum_{k=1}^{N-1}\left[2I_y^{\alpha,k}I_y^{\alpha,k+1} - \left(I_x^{\alpha,k}I_x^{\alpha,k+1} + I_z^{\alpha,k}I_z^{\alpha,k+1}\right)\right]\right\}. \tag{A10}$$

In the same way, we calculate the others $\tilde{H}_j$.

To $\tilde{H}_2$:

$$\tilde{H}_2 = \sum_{\alpha=a,b}\left\{J_{ch}S_z I_z^{\alpha,1} + J_{hh}\sum_{k=1}^{N-1}\left[2I_z^{\alpha,k}I_z^{\alpha,k+1} - \left(I_x^{\alpha,k}I_x^{\alpha,k+1} + I_y^{\alpha,k}I_y^{\alpha,k+1}\right)\right]\right\}. \tag{A11}$$

To $\tilde{H}_3$:

$$\tilde{H}_3 = \sum_{\alpha=a,b}\left\{J_{ch}S_x I_x^{\alpha,1} + J_{hh}\sum_{k=1}^{N-1}\left[2I_x^{\alpha,k}I_x^{\alpha,k+1} - \left(I_z^{\alpha,k}I_z^{\alpha,k+1} + I_y^{\alpha,k}I_y^{\alpha,k+1}\right)\right]\right\}, \tag{A12}$$

and to $\tilde{H}_4$:

$$\tilde{H}_4 = \sum_{\alpha=a,b}\left\{J_{ch}S_z I_z^{\alpha,1} + J_{hh}\sum_{k=1}^{N-1}\left[2I_z^{\alpha,k}I_z^{\alpha,k+1} - \left(I_x^{\alpha,k}I_x^{\alpha,k+1} + I_y^{\alpha,k}I_y^{\alpha,k+1}\right)\right]\right\}. \tag{A13}$$

Since $t = \sum_{k=1}\Delta t_k = 4\Delta t$, we can rewrite Eq. (A3) as

$$\bar{H}_0 = \frac{1}{4\Delta t}(\Delta t\tilde{H}_1 + \Delta t\tilde{H}_2 + \Delta t\tilde{H}_3 + \Delta t\tilde{H}_4), \tag{A14}$$

$$\bar{H}_0 = \frac{\Delta t}{4\Delta t}(\tilde{H}_1 + \tilde{H}_2 + \tilde{H}_3 + \tilde{H}_4), \tag{A15}$$

$$\bar{H}_0 = \frac{1}{4}(\tilde{H}_1 + \tilde{H}_2 + \tilde{H}_3 + \tilde{H}_4). \tag{A16}$$

Finally, replacing Eqs. (A10)–(A13) in Eq. (A16), we will have

$$\bar{H}_0 = \sum_{\alpha=a,b}\left[\frac{1}{4}J_{ch}\left(S_y I_y^{\alpha,1} + 2S_z I_z^{\alpha,1} + S_x I_x^{\alpha,1}\right) + \frac{1}{4}J_{hh}\sum_{k=1}^{N-1}\left(2I_z^{\alpha,k}I_z^{\alpha,k+1} - I_x^{\alpha,k}I_x^{\alpha,k+1} - I_y^{\alpha,k}I_y^{\alpha,k+1}\right)\right]. \tag{A17}$$

Therefore, we arrive at the effective Hamiltonian equation of the interactions between the system-environment and the environment-environment:

$$H_{\text{eff}} = H_{\text{eff}}^{SE} + H_{\text{eff}}^{E}, \tag{A18}$$

where

$$H_{\text{eff}}^{SE} = J_{ch}^{\text{eff}}\sum_{j=1}^{n}\left(2S_z I_z^j + S_x I_x^j + S_y I_y^j\right), \tag{A19}$$

$$H_{\text{eff}}^{E} = J_{hh}^{\text{eff}}\sum_{i}^{2N}\left[2I_z^i I_z^{i+1} - \left(I_x^i I_x^{i+1} + I_y^i I_y^{i+1}\right)\right], \tag{A20}$$

where $J_{ch}^{\text{eff}} = J_{ch}/4$ and $J_{hh}^{\text{eff}} = J_{hh}/4$ are, respectively, the effective coupling constants of the interactions between the ^{13}C nuclear spin and its first neighboring hydrogens and among all nuclear spins of the hydrogens in the spin chain.

The effective Hamiltonian fails at long Δt due to decoherence effects (natural relaxation of the spins) in addition to errors associated with the calibration of the pulse intensities. This could also be due to the finite size of our reservoir (hydrogen chains), but this was not investigated. In Fig. 6 we plot the magnetization of the carbon spin in the z direction ($M_z = \langle S_z\rangle$) as a function of time, derived by solving numerically the Schrödinger equation, either using the effective Hamiltonian

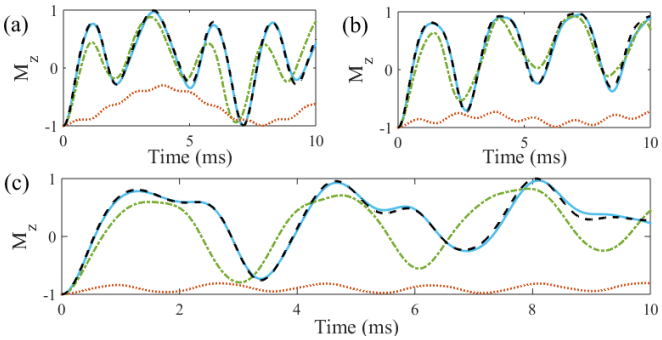

FIG. 6. Time evolution of the z component of the magnetization of the carbon nuclear spin (M_z) coupled to two symmetric chains containing a total of (a) 6, (b) 8, and (c) 10 spins of hydrogen. The dashed black line was derived using H_{eff} while the red (dotted), green (dashed-dotted), and blue (solid) lines refer to the simulations of 100 ($\Delta t = 15.10\ \mu$s), 225 ($\Delta t = 1.228\ \mu$s) and 250 ($\Delta t = 0.10\ \mu$s) cycles, respectively, with pulse sequence described by Eq. (A1). The parameters used are $\tau_p = 9.89\ \mu$s, $J_{ch}^{\text{eff}} = 550$ rad s^{-1}, $J_{hh}^{\text{eff}} = 980$ rad s^{-1}. The initial state is $|1\rangle$ for the carbon nuclear spin and $|0\rangle$ for all hydrogen spins.

and different times of free evolution. We considered the initial state of the system as $|1\rangle$ (excited) for the carbon nuclear spin and $|0\rangle$ (ground) for all hydrogen nuclear spins. We can observe that the shorter the time interval Δt, the better the match between the results predicted via H_{eff} and those obtained from the pulse sequence described by Eq. (A1), this occurs because the effects of inconsistency can be reduced when we reduce the cycle time τ_c, as τ_p is a fixed time, we can optimize Δt obtain less decoherence effect.

APPENDIX B: PROCESS MATRIX

A slight difference between experimental and theoretical data can be observed in different regions in all panels of Fig. 3. The origin of these errors are mainly due to r.f. pulse imperfections and the natural relaxation of the spins. In NMR, the thermal relaxation time is associated with the spin-lattice relaxation that occurs at a characteristic times T_1, which for our system are $T_1^{\text{H}} = 0.9$ s and $T_1^{\text{C}} = 1.6$ s. Below we discuss how these source of errors may reduce the fidelity $\mathscr{F}$ [35], which is a parameter commonly used to quantify the performance of quantum operations by checking the compatibility between experimental and theoretical operators. We can map a process matrix into a set of transformations of unitary evolutions from the initial and final density matrices [36]. For this purpose we use the equation

$$\rho_f = \sum_{mn} \chi_{mn} E_m \rho_i E_n^{\dagger}, \tag{B1}$$

where ρ_i and ρ_f are the density matrices at the beginning and end of the process, and the operators $E_m = I, S_x, -S_y, iS_z$ must form a basis. Thus the propagator χ_{mn} for the process can therefore be quantified.

We performed a quantum tomography process of the thermalized states of carbon in the situations described in Figs. 3(a) and 3(b) and from these topographies, we calculate the propagator χ_{mn}. The fidelity $\mathscr{F}$ between the experimental and ideal matrices of the thermalization process at negative temperature, Figs. 7(a) and 7(b), and of the thermalization process at positive temperature, Figs. 7(c) and 7(d), are 0.999 and 0.984, respectively.

APPENDIX C: CALCULATION OF $\langle W \rangle$ AND $\langle Q \rangle$

The quantum thermal machine proposed in this paper can be described by the relationship

$$\rho_0 \overset{\text{thermalization}}{\longrightarrow} \rho_1 \overset{U(\tau)}{\longrightarrow} \rho_2 \overset{\text{thermalization}}{\longrightarrow} \rho_1, \tag{C1}$$

and it consists of two steps that start after the qubit system has already thermalized with the reservoir, so the machine has already absorbed the heat from the reservoir. Therefore, we assume the step $\rho_0 \to \rho_1$ described by the relationship (C1) has already been performed. The cycle steps that are described in Fig. 4(a) are

Step 1: Unitary evolution applied after the qubit system has thermalized with the thermal reservoir [step $\rho_1 \to \rho_2$ in the relationship (C1)]. Therefore, a unitary evolution operator $U(\tau)$ is applied taking the ^{13}C spin state, will initially be in a thermal state equivalent to $\rho_1 = e^{-\beta_1 H_1}/Z_1$ to $\rho_2 = U(\tau)\rho_1 U^{\dagger}(\tau)$, in this step the spin temperature will depend on the unitary operator applied. $H_1 = -\frac{1}{2}\hbar\omega_1 S_z$ is Zeeman Hamiltonian, $\hbar$ being Planck's constant, ω_1 is the Larmor frequency of the ^{13}C nuclear spin, Z_1 is the partition function, and $\beta_1 = 1/k_B T$ such that $T < 0$ is the spin temperature, and k_B is the Boltzmann constant. The Hamiltonian H_1 changes in this process, which is the process where we can extract work from the machine, returning to its initial form at the end of this stage. As our unitary evolution is very fast, there is no heat exchange with the reservoir and any variation of the energy of the carbon spin will be due to the work done by it. Therefore, the Hamiltonian starts from the Hamiltonian H_1, assumes a different value $H(t)$, and then returns to H_1. In this process the entire system density operator changes (only due to the unitary evolution) and we can then calculate the energy variation due to the work performed by the system. In this case, ΔE being the variation of the energy of the machine, we have

$$\langle W \rangle = \text{Tr}(\rho_2 H_1) - \text{Tr}(\rho_1 H_1). \tag{C2}$$

Step 2: Thermalization with hot thermal reservoir [step $\rho_2 \to \rho_1$ in the relationship (C1)], when the qubit absorbs heat and then goes back to the state ρ_1. Here the Hamiltonian H_1 remains unchanged. In this case, the variation of the energy of the system is entirely due to the heat exchange [28] so that

$$\langle Q \rangle = \text{Tr}(\rho_1' H_1) - \text{Tr}(\rho_2 H_1). \tag{C3}$$

In Fig. 4 we show the application of different unitary operators: (b) $U_x = \exp(-i\frac{\pi}{2}S_x)$, (c) $U_y = \exp(-i\frac{\pi}{2}S_y)$, and (d) $U_\pi = \exp(-i\pi S_x)$, where U_x and U_y are operators that represent pulses in the x and y directions, allowing the ^{13}C spin to flip by an angle of $\pi/2$. U_π is the operator which rotates the spin by an angle of π. We also performed another unitary transformation (not shown in Fig. 4), U_I, which is an identity operator (a complete rotation around the Bloch sphere).

For the partition function we have

$$Z_1 = \text{Tr}(e^{-\beta_1 H_1}) = \langle 1|e^{-\beta_1 H_1}|1\rangle + \langle 0|e^{-\beta_1 H_1}|0\rangle \tag{C4}$$

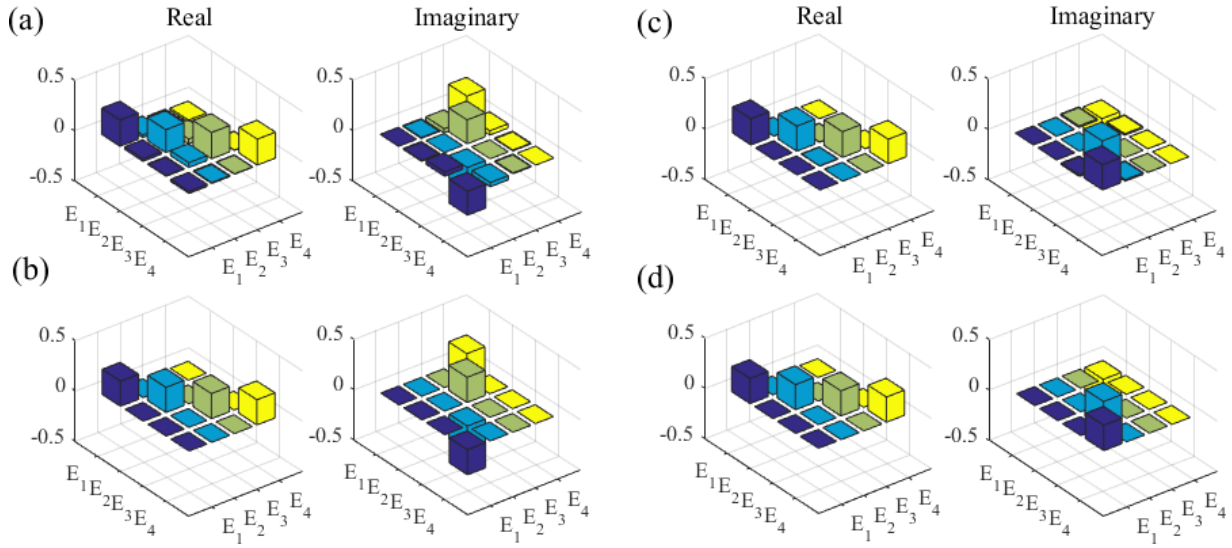

FIG. 7. Theoretical and experimental process matrices of χ_{mn} of the thermalization processes of the Figs. 3(a) and 3(b) and $E_m = I, S_x, -S_y, iS_z$. The panels on the left (right) are the real (imaginary) part. Panels (a) and (b) are, respectively, the experimental and theoretical process matrices of the Fig. 3(b). Panels (c) and (d) are, respectively, the experimental and theoretical process matrices of the Fig. 3(a).

with

$$H_1|1\rangle = \tfrac{1}{2}\hbar\omega_1|1\rangle \tag{C5}$$

and

$$H_1|0\rangle = -\tfrac{1}{2}\hbar\omega_1|0\rangle \tag{C6}$$

where $|0\rangle$ and $|1\rangle$ are, respectively, the fundamental and excited states referring to the base of the Hamiltonian $H_1(S_z)$. Then the partition function becomes

$$Z_1 = e^{\beta_1\hbar\omega_1/2} + e^{-\beta_1\hbar\omega_1/2} = 2\cosh\left(\tfrac{1}{2}\beta_1\hbar\omega_1\right). \tag{C7}$$

We will also have

$$\mathrm{Tr}(\rho_1 H_1) = \frac{1}{Z_1}\mathrm{Tr}(e^{-\beta_1 H_1}H_1), \tag{C8}$$

$$\mathrm{Tr}(\rho_1 H_1) = \frac{1}{Z_1}(\langle 1|e^{-\beta_1 H_1}H_1|1\rangle + \langle 0|e^{-\beta_1 H_1}H_1|0\rangle), \tag{C9}$$

$$\mathrm{Tr}(\rho_1 H_1) = \frac{\hbar\omega_1}{2Z_1}(\langle 1|e^{-\beta_1 H_1}|1\rangle - \langle 0|e^{-\beta_1 H_1}|0\rangle), \tag{C10}$$

$$\mathrm{Tr}(\rho_1 H_1) = \frac{\hbar\omega_1}{2Z_1}(e^{-\beta_1\hbar\omega_1/2} - e^{\beta_1\hbar\omega_1/2}), \tag{C11}$$

$$\mathrm{Tr}(\rho_1 H_1) = -\frac{\hbar\omega_1}{2}\frac{\sinh\left(\frac{1}{2}\beta_1\hbar\omega_1\right)}{\cosh\left(\frac{1}{2}\beta_1\hbar\omega_1\right)}, \tag{C12}$$

$$\mathrm{Tr}(\rho_1 H_1) = -\frac{\hbar\omega_1}{2}\tanh\left(\frac{1}{2}\beta_1\hbar\omega_1\right), \tag{C13}$$

and

$$\mathrm{Tr}(\rho_2 H_1) = \mathrm{Tr}(U(\tau)\rho_1 U^\dagger(\tau)H_1), \tag{C14}$$

$$\mathrm{Tr}(\rho_2 H_1) = \mathrm{Tr}(\rho_1 U^\dagger(\tau)H_1 U(\tau)), \tag{C15}$$

$$\mathrm{Tr}(\rho_2 H_1) = \frac{1}{Z_1}\mathrm{Tr}(e^{-\beta_1 H_1}U^\dagger(\tau)H_1 U(\tau)), \tag{C16}$$

$$\mathrm{Tr}(\rho_2 H_1) = \frac{1}{Z_1}(\langle 1|e^{-\beta_1 H_1}U^\dagger(\tau)H_1 U(\tau)|1\rangle + \langle 0|e^{-\beta_1 H_1}U^\dagger(\tau)H_1 U(\tau)|0\rangle), \tag{C17}$$

$$\mathrm{Tr}(\rho_2 H_1) = \frac{1}{Z_1}(e^{-\beta_1\hbar\omega_1/2}\langle 1|U^\dagger(\tau)H_1 U(\tau)|1\rangle + e^{\beta_1\hbar\omega_1/2}\langle 0|U^\dagger(\tau)H_1 U(\tau)|0\rangle), \tag{C18}$$

$$\mathrm{Tr}(\rho_2 H_1) = \frac{1}{Z_1}[(e^{\beta_1\hbar\omega_1/2} - e^{-\beta_1\hbar\omega_1/2})\langle 0|U^\dagger(\tau)H_1 U(\tau)|0\rangle + e^{-\beta_1\hbar\omega_1/2}\langle 0|U^\dagger(\tau)H_1 U(\tau)|0\rangle + e^{-\beta_1\hbar\omega_1/2}\langle 1|U^\dagger(\tau)H_1 U(\tau)|1\rangle], \tag{C19}$$

$$\mathrm{Tr}(\rho_2 H_1) = \frac{1}{Z_1}[(e^{\beta_1\hbar\omega_1/2} - e^{-\beta_1\hbar\omega_1/2})\langle 0|U^\dagger(\tau)H_1 U(\tau)|0\rangle + e^{-\beta_1\hbar\omega_1/2}\mathrm{Tr}(U^\dagger(\tau)H_1 U(\tau))], \tag{C20}$$

where

$$\mathrm{Tr}(U^\dagger(\tau)H_1 U(\tau)) = \mathrm{Tr}(U(\tau)U^\dagger(\tau)H_1) = \mathrm{Tr}(H_1), \tag{C21}$$

so

$$\mathrm{Tr}(H_1) = \mathrm{Tr}\left(-\tfrac{1}{2}\hbar\omega_1 S_z\right) = 0. \tag{C22}$$

Therefore,

$$\mathrm{Tr}(\rho_2 H_1) = \frac{2\sinh\left(\frac{1}{2}\beta_1\hbar\omega_1\right)}{2\cosh\left(\frac{1}{2}\beta_1\hbar\omega_1\right)}\langle 0|U^\dagger(\tau)H_1 U(\tau)|0\rangle, \tag{C23}$$

$$\mathrm{Tr}(\rho_2 H_1) = \tanh\left(\frac{1}{2}\beta_1\hbar\omega_1\right)\langle 0|U^\dagger(\tau)H_1 U(\tau)|0\rangle, \tag{C24}$$

$$\mathrm{Tr}(\rho_2 H_1) = \tanh\left(\frac{1}{2}\beta_1\hbar\omega_1\right)\langle 0|U^\dagger(\tau)H_1 * (|0\rangle\langle 0| + |1\rangle\langle 1|)U(\tau)|0\rangle, \tag{C25}$$

$$\mathrm{Tr}(\rho_2 H_1) = -\frac{1}{2}\hbar\omega_1 \tanh\left(\frac{1}{2}\beta_1\hbar\omega_1\right)[\langle 0|U^\dagger(\tau) * (|0\rangle\langle 0| - |1\rangle\langle 1|)U(\tau)|0\rangle], \quad \text{(C26)}$$

$$\mathrm{Tr}(\rho_2 H_1) = -\frac{1}{2}\hbar\omega_1 \tanh\left(\frac{1}{2}\beta_1\hbar\omega_1\right)[\langle 0|U^\dagger(\tau) * (\mathbb{I} - 2|1\rangle\langle 1|)U(\tau)|0\rangle], \quad \text{(C27)}$$

$$\mathrm{Tr}(\rho_2 H_1) = -\frac{1}{2}\hbar\omega_1 \tanh\left(\frac{1}{2}\beta_1\hbar\omega_1\right)[\langle 0|U^\dagger(\tau)U(\tau)|0\rangle - 2\langle 0|U^\dagger(\tau)|1\rangle\langle 1|U(\tau)|0\rangle], \quad \text{(C28)}$$

$$\mathrm{Tr}(\rho_2 H_1) = -\frac{1}{2}\hbar\omega_1 \tanh\left(\frac{1}{2}\beta_1\hbar\omega_1\right) * \left[1 - 2|\langle 1|U(\tau)|0\rangle|^2\right], \quad \text{(C29)}$$

where $\xi = |\langle 1|U(\tau)|0\rangle|^2$ is the probability of transition between states $|0\rangle$ and $|1\rangle$. Therefore,

$$\mathrm{Tr}(\rho_2 H_1) = -\frac{\hbar\omega_1}{2}\tanh\left(\frac{1}{2}\beta_1\hbar\omega_1\right)[1 - 2\xi^2]. \quad \text{(C30)}$$

Replacing Eqs. (C13) and (C30) in Eqs. (C2) and (C3):

$$\langle W\rangle = -\frac{\hbar\omega_1}{2}\tanh\left(\frac{1}{2}\beta_1\hbar\omega_1\right)[1 - 2\xi^2] + \frac{\hbar\omega_1}{2}\tanh\left(\frac{1}{2}\beta_1\hbar\omega_1\right), \quad \text{(C31)}$$

so

$$\langle W\rangle = \xi^2\hbar\omega_1\tanh\left(\tfrac{1}{2}\beta_1\hbar\omega_1\right) \quad \text{(C32)}$$

and

$$\langle Q\rangle = -\frac{\hbar\omega_1}{2}\tanh\left(\frac{1}{2}\beta_1\hbar\omega_1\right) + \frac{\hbar\omega_1}{2}\tanh\left(\frac{1}{2}\beta_1\hbar\omega_1\right)[1 - 2\xi^2], \quad \text{(C33)}$$

so

$$\langle Q\rangle = -\xi^2\hbar\omega_1\tanh\left(\tfrac{1}{2}\beta_1\hbar\omega_1\right). \quad \text{(C34)}$$

Efficiency is defined as $\eta = -\langle W\rangle/\langle Q\rangle$.

(i) When $\xi = 0$, $\langle W\rangle = 0$, and $\langle Q\rangle = 0$. In this case, the thermal machine will have same initial and final states after unitary operation. There is no work nor heat exchange in this case.

(ii) When $\xi > 0$ and $\beta > 0$, $\langle W\rangle = \xi^2\hbar\omega_1\tanh(\frac{1}{2}\beta_1\hbar\omega_1) > 0$ and $\langle Q\rangle = -\xi^2\hbar\omega_1\tanh(\frac{1}{2}\beta_1\hbar\omega_1) < 0$, the machine will always turn all net work into heat when it comes in contact with the hot reservoir.

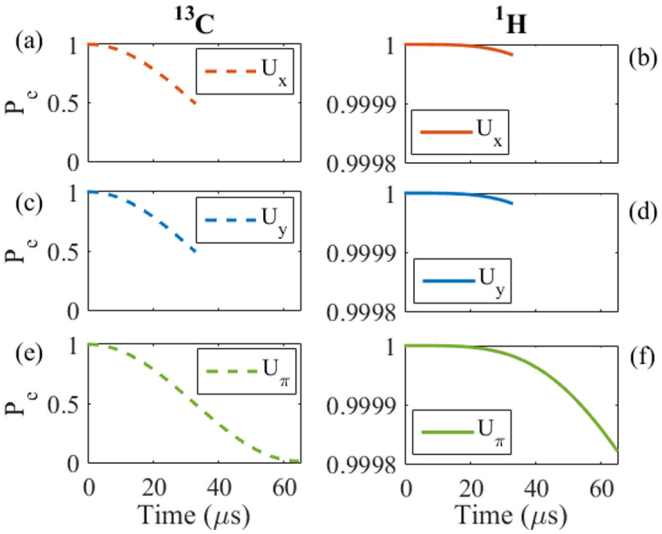

FIG. 8. Population of the excited state (P_e) versus pulse time of the unitary evolutions U_x (a) and (b), U_y (c) and (d), and U_π (e) and (f). (a), (c), and (e) show the effect of the operation on the ^{13}C spin while (b), (d), and (f) show the same effect (on average) on the hydrogen spins.

(iii) When $\xi > 0$ and $\beta < 0$, $\langle W\rangle = \xi^2\hbar\omega_1\tanh(\frac{1}{2}\beta_1\hbar\omega_1) < 0$ and $\langle Q\rangle = -\xi^2\hbar\omega_1\tanh(\frac{1}{2}\beta_1\hbar\omega_1) > 0$, the thermal machine always turns all absorbed heat from the hot reservoir into net work. Thus, here we have a thermal machine with maximum efficiency.

APPENDIX D: RESERVOIR ENERGY LOSS

To check if there is gain or loss of energy from the hydrogen bath during the unitary evolution applied in each cycle, we simulate the application of an r.f. pulse in the ^{13}C after its thermalization with the reservoir (proposed step in our cycle). In Fig. 8 we show the influence of unitary evolution in the population of the excited state of the system qubit (carbon) and the average under the spins of the reservoir (hydrogens).

The ^{13}C magnetization in the x, y, and z directions, $M_U = (M_x, M_y, M_z)$, immediately after each unitary operation is $M_{U_x} = (0.08, -0.99, 0.00)$a.u. [Fig. 8(a)], $M_{U_y} = (0.99, 0.08, 0.00)$a.u. [Fig. 8(c)] and $M_{U_\pi} = (0.17, -0.01, 0.98)$a.u. [Fig. 8(e)]. In Figs. 8(b), 8(d), and 8(f) we see the average populations of the excited states of the hydrogen chain of the spin chain immediately after each unitary evolution. In the simulations we used two chains with 10 hydrogen spins each. We observed that the energy loss always occurs for the first two spins in the chain (spins closer to ^{13}C). The greatest loss of energy from the spin bath occurs for the unit operation corresponding to an evolution of π (U_π), and such loss corresponds to 0.4% of the value before the operation. We conclude, then, that the unitary evolution occur fast enough so that there is no significant loss of energy caused by the exchange interaction between the system qubit and the spin reservoir.

[1] J. Gemmer, M. Michel, and G. Mahler, *Quantum Thermodynamics* (Springer Verlag, Berlin, 2004).

[2] R. Alicki, The quantum open system as a model of the heat engine, J. Phys. A **12**, L103 (1979).

[3] H. T. Quan, Yu-xi Liu, C. P. Sun, and Franco Nori, Quantum thermodynamic cycles and quantum heat engines, Phys. Rev. E **76**, 031105 (2007).

[4] E. M. Purcell and R. V. Pound, A nuclear spin system at negative temperature, Phys. Rev. **81**, 279 (1951).

[5] N. F. Ramsey, Thermodynamics and statistical mechanics at negative absolute temperatures, Phys. Rev. **103**, 20 (1956).

[6] L. D. Carr, Negative temperatures? Science **339**, 42 (2013).

[7] S. Braun, J. P. Ronzheimer, M. Schreiber, S. S. Hodgman, T. Rom, I. Bloch, and U. Schneider, Negative absolute temperature for motional degrees of freedom, Science **339**, 52 (2013).

[8] R. J. de Assis, T. M. de Mendonça, C. J. Villas-Boas, A. M. de Souza, R. S. Sarthour, I. S. Oliveira, and N. G. de Almeida, Efficiency of a Quantum Otto Heat Engine Operating Under a Reservoir at Effective Negative Temperatures, Phys. Rev. Lett. **122**, 240602 (2019).

[9] J. F. Poyatos, J. I. Cirac, and P. Zoller, Quantum Reservoir Engineering with Laser Cooled Trapped Ions, Phys. Rev. Lett. **77**, 4728 (1996).

[10] C. J. Myatt, B. E. King, Q. A. Turchette, C. A. Sackett, D. Kielpinski, W. M. Itano, C. Monroe, and D. J. Wineland, Decoherence of quantum superpositions through coupling to engineered reservoirs, Nature (London) **403**, 269 (2000).

[11] K. W. Murch, S. J. Weber, K. M. Beck, E. Ginossar, and I. Siddiqi, Reduction of the radiative decay of atomic coherence in squeezed vacuum, Nature (London) **499**, 62 (2013).

[12] A. R. R. Carvalho, P. Milman, R. L. de Matos Filho, and L. Davidovich, Decoherence, Pointer Engineering, and Quantum State Protection, Phys. Rev. Lett. **86**, 4988 (2001).

[13] T. Werlang, R. Guzmán, F. O. Prado, and C. J. Villas-Bôas, Generation of decoherence-free displaced squeezed states of radiation fields and a squeezed reservoir for atoms in cavity qed, Phys. Rev. A **78**, 033820 (2008).

[14] S. Pielawa, G. Morigi, D. Vitali, and L. Davidovich, Generation of Einstein-Podolsky-Rosen-Entangled Radiation through an Atomic Reservoir, Phys. Rev. Lett. **98**, 240401 (2007).

[15] T. Werlang and C. J. Villas-Boas, Theoretical method for the generation of a dark two-mode squeezed state of a trapped ion, Phys. Rev. A **77**, 065801 (2008).

[16] F. O. Prado, E. I. Duzzioni, M. H. Y. Moussa, N. G. de Almeida, and C. J. Villas-Bôas, Nonadiabatic Coherent Evolution of Two-Level Systems Under Spontaneous Decay, Phys. Rev. Lett. **102**, 073008 (2009).

[17] F. Verstraete, M.l M. Wolf, and J. Ignacio Cirac, Quantum computation and quantum-state engineering driven by dissipation, Nat. Phys. **5**, 633 (2009).

[18] Y. Hama, W. J. Munro, and K. Nemoto, Relaxation to Negative Temperatures in Double Domain Systems, Phys. Rev. Lett. **120**, 060403 (2018).

[19] M. Lovrić, H. G. Krojanski, and D. Suter, Decoherence in large quantum registers under variable interaction with the environment, Phys. Rev. A **75**, 042305 (2007).

[20] G. A. Álvarez and D. Suter, Measuring the Spectrum of Colored Noise by Dynamical Decoupling, Phys. Rev. Lett. **107**, 230501 (2011).

[21] G. A. Alvarez, A. Ajoy, X. Peng, and D. Suter, Performance comparison of dynamical decoupling sequences for a qubit in a rapidly fluctuating spin bath, Phys. Rev. A **82**, 042306 (2010).

[22] A. Ajoy, G. A. Alvarez, and D. Suter, Optimal pulse spacing for dynamical decoupling in the presence of a purely dephasing spin bath, Phys. Rev. A **83**, 032303 (2011).

[23] A. M. Souza, G. A. Alvarez, and D. Suter, Robust Dynamical Decoupling for Quantum Computing and Quantum Memory, Phys. Rev. Lett. **106**, 240501 (2011).

[24] A. Abragam, *Principles of Nuclear Magnetism* (Oxford University Press, Oxford, 1962).

[25] C. P. Slichter, *Principles of Magnetic Resonance*, Vol. 3 (Springer, Berlin, 1990).

[26] H. Struchtrup, Work Storage in States of Apparent Negative Thermodynamic Temperature, Phys. Rev. Lett. **120**, 250602 (2018).

[27] W. K. Wootters, Entanglement of Formation of an Arbitrary State of Two Qubits, Phys. Rev. Lett. **80**, 2245 (1998).

[28] J. Anders and V. Giovannetti, Thermodynamics of discrete quantum processes, New J. Phys. **15**, 033022 (2013).

[29] M. O. Scully, M. Suhail Zubairy, G. S. Agarwal, and H. Walther, Extracting work from a single heat bath via vanishing quantum coherence, Science **299**, 862 (2003).

[30] P. A. Camati, J. F. G. Santos, and R. M. Serra, Coherence effects in the performance of the quantum otto heat engine, Phys. Rev. A **99**, 062103 (2019).

[31] J. Klaers, S. Faelt, A. Imamoglu, and E. Togan, Squeezed Thermal Reservoirs as a Resource for a Nanomechanical Engine Beyond the Carnot Limit, Phys. Rev. X **7**, 031044 (2017).

[32] John P. S. Peterson, T. B. Batalhão, M. Herrera, A. M. Souza, R. S. Sarthour, I. S. Oliveira, and R. M. Serra, Experimental Characterization of a Spin Quantum Heat Engine, Phys. Rev. Lett. **123**, 240601 (2019).

[33] W. Magnus, On the exponential solution of differential equations for a linear operator, Commun. Pure Appl. Math. **7**, 649 (1954).

[34] M. M. Maricq, Application of average hamiltonian theory to the nmr of solids, Phys. Rev. B **25**, 6622 (1982).

[35] X. Wang, C. S. Yu, and X. X. Yi, An alternative quantum fidelity for mixed states of qudits, Phys. Lett. A **373**, 58 (2008).

[36] I. L. Chuang and M. A. Nielsen, Prescription for experimental determination of the dynamics of a quantum black box, J. Mod. Opt. **44**, 2455 (1997).